

Modeling aggregation processes of Lennard-Jones particles via stochastic networks

Yakir Forman¹ and Maria Cameron²

December 9, 2024

Abstract

We model an isothermal aggregation process of particles/atoms interacting according to the Lennard-Jones pair potential by mapping the energy landscapes of each cluster size N onto stochastic networks, computing transition probabilities for the network for an N -particle cluster to the one for $N + 1$, and connecting these networks into a single joint network. The attachment rate is a control parameter. The resulting network representing the aggregation of up to 14 particles contains 6417 vertices. It is not only time-irreversible but also reducible. To analyze its transient dynamics, we introduce the sequence of the expected initial and pre-attachment distributions and compute them for a wide range of attachment rates and three values of temperature. As a result, we find the most likely to observe configurations in the process of aggregation for each cluster size. We examine the attachment process and conduct a structural analysis of the sets of local energy minima for every cluster size. We show that both processes taking place in the network, attachment and relaxation, lead to the dominance of icosahedral packing in small (up to 14 atom) clusters.

1 Introduction

This work is inspired by the gap between theoretical studies of clusters of Lennard-Jones atoms and experimental works where rare gas clusters are examined by means of electron [12, 13, 14, 17, 18] or X-ray [23] diffraction. The former ones achieved significant progress in understanding thermodynamics (e.g. Refs [7, 26]) and transition processes (e.g. Refs. [31, 28, 33, 34]) of/in clusters of *fixed* numbers of particles, while rare gas atoms self-assemble into clusters in experimental settings, and *nothing prevents them from acquiring new atoms*. Mass spectra measured in experimental work [12, 13, 14, 17, 18] provide a strong evidence that icosahedral clusters tend to form with small numbers of atoms, while face-centered cubic (FCC) packing becomes prevalent for large clusters. The switch from icosahedral to FCC packing occurs somewhere in the range of cluster size from 1500 to 10^4 atoms, while the presence of FCC packing was detected in clusters of $N \geq 200$ atoms [23]. What is the mechanism of this switch? Van de Waal hypothesized that this switch happens not due to rearrangement of atoms within clusters but because faulty FCC layers start to grow on icosahedral cores [32]. Kovalenko et al [24] inferred the structure of large rare gas clusters from experimental measurements and showed that it was consistent with Van de Waal's conjecture.

¹yakir.forman@mail.yu.edu, Yeshiva University, 500 W 185th St, New York, NY 10033

²cameron@math.umd.edu, Department of Mathematics, University of Maryland, College Park, MD 20742

1.1 Intriguing facts about the self-assembly of free Lennard-Jones atoms

The potential energy of a cluster of N particles interacting according to the Lennard-Jones pair potential written in reduced units is given by

$$V(\mathbf{r}_1, \dots, \mathbf{r}_N) = 4 \sum_{i=2}^N \sum_{j=1}^i (r_{ij}^{-12} - r_{ij}^{-6}), \quad r_{ij} = |\mathbf{r}_i - \mathbf{r}_j|, \quad \mathbf{r}_i = (x_i, y_i, z_i). \quad (1)$$

The global energy minima for cluster sizes $2 \leq N \leq 110$ are mostly achieved on configurations with icosahedral packing; however, for some special numbers of atoms, $N = 38, 75, 76, 77, 102, 103,$ and 104 , the energy-minimizing configurations are non-icosahedral [30]. Some of them are highly symmetric. For example, the global minimum for $N = 38$, a truncated octahedron with the FCC atomic packing, has the point group O_h of order 48, i.e., there are 48 orthogonal transformations mapping the cluster onto itself. The global minimum for $N = 75$, a Marks decahedron, has point group D_{5h} of order 20. Remarkably, the mass spectra graphs in [12, 17] do not have prominent peaks at $N = 38$ and $N = 75$ which suggests that the highly symmetric global minima for these numbers of atoms are not found by nature if new atoms are allowed to arrive and/or the temperature is too high. On the other hand, the mass spectra in [12, 13, 14, 17, 18] consistently exhibit peaks corresponding to the clusters of the so-called magic numbers of atoms N admitting complete icosahedra. These numbers are: $N = 13, 55, 147, 309, 561, \dots$. The point group order of an icosahedron is 120. Evidently, the atoms tend to self-assemble into complete icosahedra despite their high symmetry and the presence of free atoms ready to glue to them.

1.2 Choosing an approach

Intrigued by these facts, we undertook an attempt to understand the self-assembly of free Lennard-Jones atoms into clusters on the quantitative level by means of combined analytical and computational methods. All previous theoretical studies of Lennard-Jones clusters dealt with those of fixed numbers of atoms, i.e., atoms were neither allowed to fly away nor join the cluster, to the best of our knowledge. These works can be divided into two groups, full phase-space-based (e.g. [26, 28]), and network-based. The latter approach was pioneered by Wales and collaborators [27, 30, 8, 33, 34]. Their powerful computational tools for mapping energy landscapes onto networks are based on the basin-hopping method [30] and discrete path sampling [31]. Numerous networks representing energy landscapes of proteins (e.g. [6]) and clusters of particles interacting according to various pair potentials (e.g. [15, 35]) are available or advertised in the Wales's group web page [36]. In this work, we choose to go along with the network-based approach due to its simplicity and visuality.

1.3 A brief summary of main results

Thus, our goal is to build a network representing the aggregation and dynamics of Lennard-Jones clusters and analyze it.

We have created such a network for up to 14 atoms. The vertices of this network represent local energy minima for each N -atom cluster, $6 \leq N \leq 14$. Energy minima that can be obtained one from another by translations, orthogonal transformations, or permutations of atoms are mapped onto the same vertex. For brevity, we will denote both, the N -atom Lennard-Jones cluster and the network representing its energy landscape, by LJ_N . In each LJ_N , the local minima are ordered in the increasing order of their potential energies. The i th lowest minimum and the corresponding state of the LJ_N network will be denoted by $MN(i)$. The energy landscapes of LJ_2, LJ_3, LJ_4 and LJ_5 are trivial as they consist of unique potential energy minima: dimer, triangle, tetrahedron, and trigonal bipyramid (bi-tetrahedron) respectively. We computed the

LJ_N networks for $N = 6, \dots, 14$ (LJ₁₃ is also available at [36]), and connected them by evaluating transition probabilities from each vertex of LJ_N to each vertex of LJ_{N+1}. The transition rate along the directed edges (a.k.a. arcs) representing such transitions is the rate of new atom arrival, or the attachment rate μ . The attachment times are assumed to be exponentially distributed random variables with the parameter μ . We did not include arcs from LJ_{N+1} to LJ_N as the transition rates along them would be rather small in the considered isothermal aggregation due to the necessity to break at least 3 bonds in order to remove an atom from a cluster.

Therefore, the resulting *aggregation/deformation LJ₆₋₁₄ network* contains two kinds of edges: undirected edges connecting vertices in each LJ_N, and directed edges (a.k.a. arcs) connecting LJ_N to LJ_{N+1}. The LJ₆₋₁₄ network is not only *time-irreversible* but also *reducible*. Its invariant probability distribution is supported only on LJ₁₄. We are interested in its transient dynamics. We pose the following question. If the aggregation process starts at M6(2), the bicapped tetrahedron local minimum of LJ₆, which arises as a result of the attachment of an additional atom to the only minimum of LJ₅, what configurations are most likely to observe in each LJ_N as the aggregation process proceeds to LJ₁₄? Time-reversibility and/or irreducibility were typically assumed in deterministic methods used for analysis of Lennard-Jones networks, e.g., the transition path theory tools [3] need strictly positive invariant distribution to evaluate reactive currents, while the eigencurrents are defined so far only for time-reversible and irreducible networks [4, 5].

In this work, we introduce so-called expected initial and pre-attachment distributions to analyze the aggregation/deformation LJ₆₋₁₄ network. Both of these distributions depend on the attachment rate μ . Assuming that an initial probability distribution for LJ_N is given, the expected pre-attachment distribution is calculated from it as the expected probability distribution at the attachment time. Having found the expected pre-attachment distribution for LJ_N, one can convert it to the expected initial probability distribution for LJ_{N+1} using the found transition probabilities along the arcs connecting LJ_N and LJ_{N+1}. Continuing this process, one can compute the whole sequence of the expected initial and pre-attachment distributions up to $N = 14$ and answer the posed question. The inspection of the computed distributions shows at which stage of the process configurations based on icosahedral packing start to dominate. In particular, the 13-atom icosahedron is the most likely configuration to observe for the 13-atom cluster for a wide range of attachment rates, from low to medium. Unsurprisingly, the capped icosahedron, the global minimum of LJ₁₄, dominates the initial and the pre-attachment distributions for LJ₁₄. The computed expected initial and pre-attachment distributions are compared to the invariant distributions, by measuring the normalized root-mean-square discrepancies introduced in this work.

The dominance of local minima based on icosahedral packing is evident from our results for $N \leq 10 \leq 14$. In order to understand the origin of icosahedral clusters, we examine the attachment process and conduct a structural analysis of local energy minima for all cluster sizes. The attachment of new atoms converts significant fractions of local minima of LJ_N with non-icosahedral packing to local minima of LJ_{N+1} with icosahedral packing for $N \leq 11 \leq 13$. Our results indicate that both processes taking place in the LJ₆₋₁₄ network, attachment and relaxation, work in favor of the formation of configurations with icosahedral packing.

The rest of the paper is organized as follows. In Section 2, we explain how the LJ₆₋₁₄ network is computed. Section 3 is devoted to the analysis of the LJ₆₋₁₄ network. We discuss some perspectives of the introduced approach for modeling aggregation processes of interacting particles in Section 4.

2 Construction of the Aggregation/Deformation LJ₆₋₁₄ network

The LJ₆₋₁₄ network consists of nine LJ_N sub-networks, $N = 6, \dots, 14$ connected by arcs representing the attachment of new atoms.

2.1 Construction of LJ_N networks

LJ₆ has two energy minima separated by a transition state, a.k.a. a Morse-index one saddle (the Morse index is the number of negative eigenvalues in the Hessian matrix). The octahedron, the global minimum M6(1) of LJ₆, can be formed only due to the structural transition in LJ₆, while the minimum M6(2), the bicapped tetrahedron, can also arise from the only minimum of LJ₅, the trigonal bipyramid, as a result of the attachment of a new atom. The LJ₇ network containing 4 vertices corresponding to the local minima and 6 transition states separating distinct vertices was presented in [27]. We used it as a checkpoint for our techniques. Since the networks LJ_N for $N \leq 14$ are relatively small, we aimed at finding the whole set of local minima for each of them. The found global minima were compared with the list in [30]. The set of minima of LJ₁₃ was taken from [36]¹. The rest of LJ_N, $6 \leq N \leq 12$, and $N = 14$ had to be generated.

The networks LJ_N for $N \geq 8$ were generated sequentially as follows. The fast and robust trust region BFGS method [29] was chosen for numerical minimization. An initial set of local minima was found by $\leq 10^4$ minimization runs starting from random initial configurations. Some more local minima were found by 10^3 hops of the basin hopping method [30] starting from each initially found minimum. A few more local minima were found as a result of the evaluation of transition probabilities from the minima of LJ_{N-1} to those of LJ_N (see Section 2.2). Finally, a few extra local minima were found as a result of our search for transition states starting from each available local minimum on the other side of the detected Morse index one saddle.

The search for transition states in each LJ_N was accomplished using the technique proposed by S. Sousa Castellanos² that combined two methods, the min-mode method (following the eigenvector associated with the smallest eigenvalue) (e.g. [11, 16]) and the shrinking dimer method [19, 37], in two `for`-loops going over certain sequences of values of two key parameters, the step size in the min-mode method, and the threshold value of the eigenvalue at which the min-mode method switches to the shrinking dimer. This technique (we named it “the saddle hunt”) has important advantages. First, the search for Morse index one saddles starts at local minima. Hence, the problems of finding an initial approximation as in the shrinking dimer method, or aligning the endpoints as in the string [9, 10] and the nudged elastic band [22] methods are eliminated, and the number of runs is equal to the number of local minima. Second, the saddle hunt method finds collections of distinct Morse index one saddles starting from the same local minimum thanks to its `for`-loops. In summary, the saddle hunt turned out to be a quite powerful technique. It will be reported in details separately.

If two local minima i and j in LJ_N are separated by a transition state s , the transition rate from i to j via s is given by Langer’s formula [25] upgraded to take the point group orders into account as in [31]:

$$L_{i \rightarrow j}^s \approx \frac{O_i |\lambda_s|}{O_s 2\pi} \sqrt{\frac{\det H_i}{|\det H_s|}} e^{-\beta(V_s - V_i)} \quad (2)$$

where λ_s is the only negative eigenvalue of the Hessian matrix at the saddle s , V_i and V_s are the potential energy values, H_i and H_s are the Hessian matrices, and O_i and O_s are the point group orders at i and s respectively. Note that the corresponding vertices i and j might be separated by multiple edges corresponding to different transition states. The total transition rate from the state i to the state j is the sum of the transition rates along all edges connecting i and j .

We developed a code that computes the point group orders in Eq. (2) for any set of points in 3D. The code makes use of the orbit-stabilizer theorem: given a group G acting on a set X , for any $i \in X$, $|G| = |\text{orb}(i)| |\text{stab}(i)|$ where $\text{orb}(i) := \{j \in X \mid gi = j \text{ for some } g \in G\}$ is the *orbit* of i , and $\text{stab}(i) := \{g \in G \mid gi = i\}$ is the *stabilizer* of i . Let X be the set of coordinates $\{\mathbf{r}_k := (x_k, y_k, z_k)\}_{k=1}^N$ of atomic centers in the cluster, and G be the point group that we want

¹The dataset for LJ₁₃ found in [36] containing 28970 Morse index one saddles significantly oversamples the set of transition states in comparison with our networks LJ_N, $N \geq 8$. Therefore, we computed the set of transition states for LJ₁₃ using our technique, so that it is sampled consistently with our networks LJ_N, $6 \leq N \leq 12$ and $N = 14$.

²S. Sousa Castellanos (East Carolina University) was M. Cameron’s MAPS-REU student in Summer 2016

to find. We choose one point $\mathbf{r}_p := (x_p, y_p, z_p)$ and first exhaustively test all possible orthogonal transformations that leave both \mathbf{r}_p and the center of mass in place, while map X onto itself. Then we exhaustively test whether the atom at \mathbf{r}_p can be mapped to each other atom at equal distance from the center of mass, while X is mapped onto itself. During both tests, we count all such transformations which map X onto itself, and thus obtain $|\text{stab}(\mathbf{r}_p)|$ and $|\text{orb}(\mathbf{r}_p)|$.

Each LJ_N network is time-reversible and irreducible. With the transition rates given by Eq. (2), its invariant distribution is a row vector π^N whose components are given by

$$\pi_i^N = \frac{e^{-V_i/T} O_i^{-1} (\det H_i)^{-1/2}}{\sum_j e^{-V_j/T} O_j^{-1} (\det H_j)^{-1/2}}, \quad (3)$$

where the sum in the denominator is taken over the whole set of vertices in LJ_N .

Fig. 1 showing the numbers of local minima for LJ_N , $6 \leq N \leq 14$ suggests that the number of local minima grows exponentially with the number of atoms. The least squares fit by an

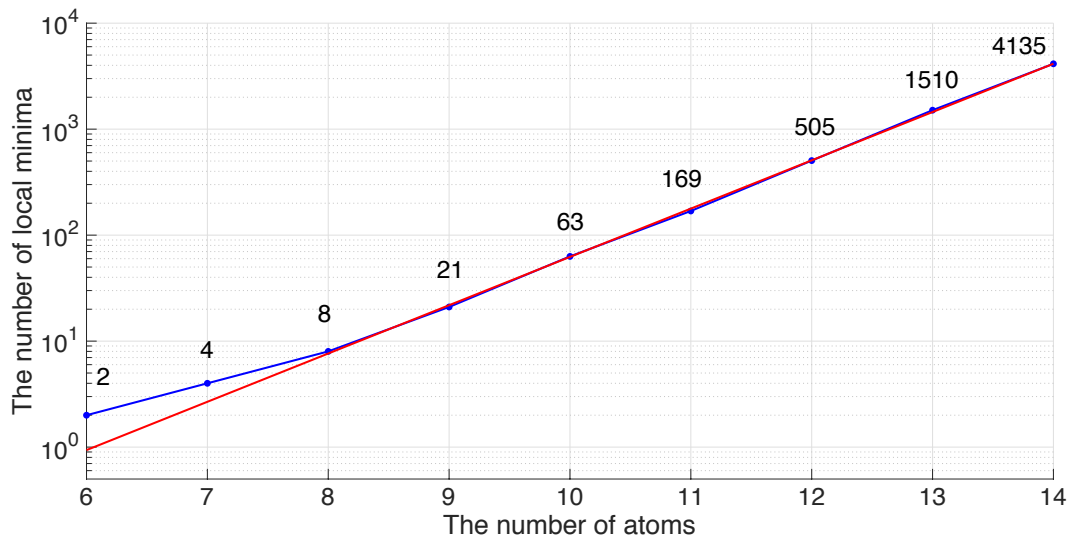


Figure 1: Blue dots: the numbers of local minima in LJ_N for $6 \leq N \leq 14$. Red line: the least squares fit (ignoring $N = 6, 7$) given by Eq. (4).

exponential function gives:

$$N_{\min}(N) = 1.7 \cdot 10^{-3} \cdot e^{1.05N}. \quad (4)$$

2.2 Connecting LJ_N and LJ_{N+1}

A new atom joining a cluster of N atoms configured near a local energy minimum i of LJ_N will cause the cluster to relax to near some local minimum j of LJ_{N+1} depending on the mutual arrangement of the N -cluster and the new atom. We need to compute the transition probabilities $\gamma_{ij}^{N \rightarrow N+1}$ that a minimum i of LJ_N will transform into a minimum j of LJ_{N+1} . Naturally, $\sum_j \gamma_{ij}^{N \rightarrow N+1} = 1$.

We propose the following method for estimating the transition probabilities. Let $U(\mathbf{r})$, $\mathbf{r} = (x, y, z)$, be the potential energy of interaction of a new atom at the location \mathbf{r} and the N -atom cluster whose atoms are at fixed locations $\{\mathbf{r}_{\mathbf{k}}\}_{\mathbf{k}=1}^N$:

$$U(\mathbf{r}) := 4 \sum_{\mathbf{k}=1}^N (|\mathbf{r} - \mathbf{r}_{\mathbf{k}}|^{-12} - |\mathbf{r} - \mathbf{r}_{\mathbf{k}}|^{-6}). \quad (5)$$

Note that $U(\mathbf{r}) \rightarrow 0$ as $|\mathbf{r}| \rightarrow \infty$. Consider the equipotential surface

$$\Sigma := \{\mathbf{r} \in \mathbb{R}^3 \mid U(\mathbf{r}) = U_0, \min_{1 \leq k \leq N} |\mathbf{r} - \mathbf{r}_k| > 2^{1/6}\}, \quad (6)$$

where U_0 is a small in absolute value negative number. In our calculations, we set $U_0 = -0.1$. The condition $\min_{1 \leq k \leq N} |\mathbf{r} - \mathbf{r}_k| > 2^{1/6}$ eliminates the components of $\{\mathbf{r} \in \mathbb{R}^3 \mid U(\mathbf{r}) = U_0\}$ (if any) lying inside Σ . An example of such an equipotential surface surrounding the M6(2) minimum of LJ₆ is shown in Fig. 2. We assume that the landing site of the new atom arriving from the outer space on the equipotential surface Σ is a uniformly distributed random variable. We surround every local minimum i of LJ_N with the equipotential surface Σ given by Eq. (6),

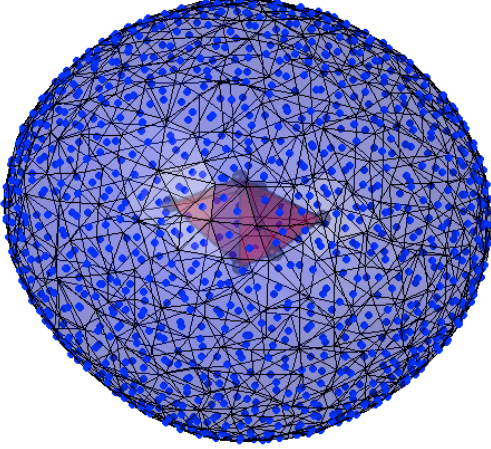


Figure 2: The equipotential surface given by Eq. (6) with $U_0 = -0.1$ surrounding the bicapped tetrahedron local minimum of LJ₆. The surface is triangulated into 1000 faces. Blue dots indicate the centers of the faces.

and triangulate it:

$$\Sigma = \bigcup_{m=1}^M \sigma_m, \quad \text{where } \sigma_m \text{'s are triangular faces.}$$

The target value of M is 1000. For each face center, we run minimization using the trust region BFGS with a small maximal trust region radius and identify the minimum j of LJ_{N+1} to which the run converges. For $N \leq 8$, it suffices to compare the energy value of the found minimum with the energies of the minima of LJ_{N+1}. For larger N , if the energy of the found minimum coincides with that of a minimum j of LJ_{N+1} up to the prescribed tolerance, we look for an orthogonal transformation that aligns the found minimum with the minimum j . The transition probability $\gamma_{ij}^{N \rightarrow N+1}$ from minimum i of LJ_N to minimum j of LJ_{N+1} is estimated using the formula:

$$\gamma_{ij}^{N \rightarrow N+1} = \frac{\sum_{m=1}^M A(\sigma_m) \delta_{ij}(m)}{A(\Sigma)}, \quad (7)$$

where $A(\sigma)$ denotes the area of σ , and $\delta_{ij}(m) = 1$ if and only if the minimization run for minimum i and face m converges to minimum j , and $\delta_{ij}(m) = 0$ otherwise.

Thus, we connect every pair of vertices i in LJ_N and j in LJ_{N+1} with the arc $(i \rightarrow j)$ whenever $\gamma_{ij}^{N \rightarrow N+1} > 0$. Given the attachment rate μ , transition rate along the arc $(i \rightarrow j)$ is $\mu \gamma_{ij}^{N \rightarrow N+1}$.

Such a connection of LJ_N and LJ_{N+1} renders the resulting Markov chain time-irreversible and reducible. Each LJ_N component except for the last one created LJ₁₄ is transient, since the attachment causes the process to leave each LJ_N to LJ_{N+1} without the possibility of return.

The created network LJ_{6-14} is visualized in Fig. 3. Each LJ_N is presented as a black disconnectivity graph [2], while selected arcs from LJ_N to LJ_{N+1} are depicted with catenary-shaped colored curves. An arc ($i \rightarrow j$) from LJ_N to LJ_{N+1} is shown if and only if i is not more than 50th lowest minimum of LJ_N and $\gamma_{ij}^{N \rightarrow N+1} > 0.1$. The statistics for the LJ_{6-14} networks

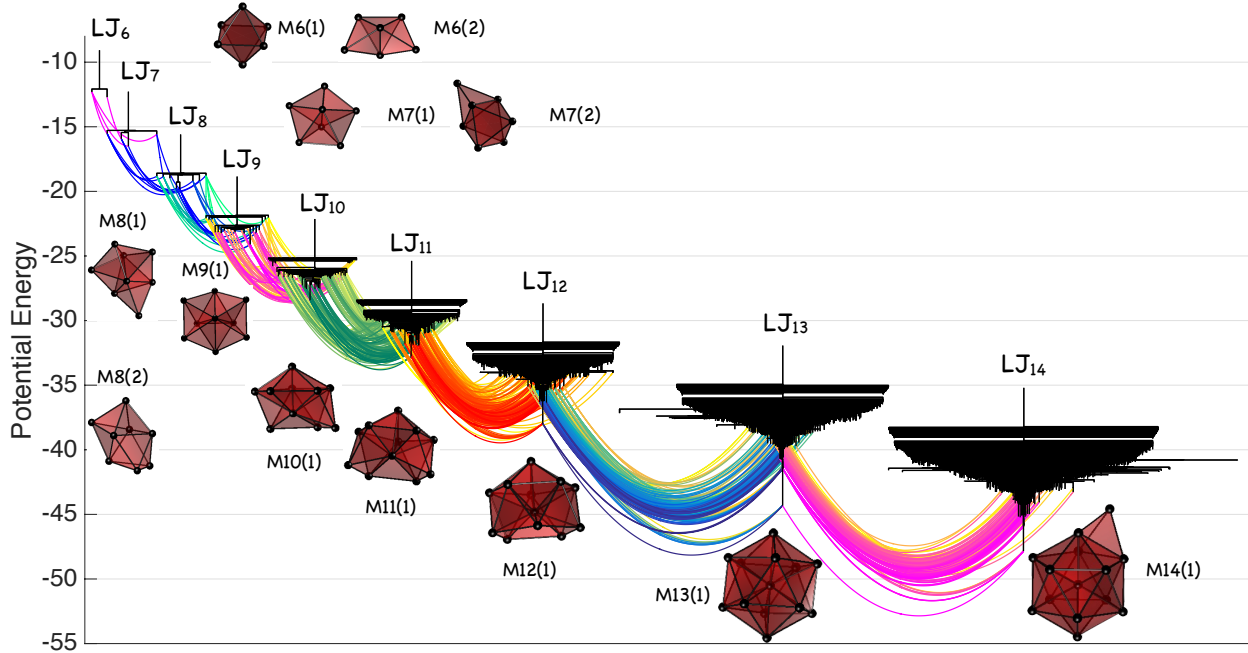


Figure 3: The LJ_{6-14} aggregation/deformation network. The components LJ_N are visualised as disconnectivity graphs, while selected arcs from LJ_N to LJ_{N+1} are depicted with catenary-shaped colored curves. An arc ($i \rightarrow j$) from LJ_N to LJ_{N+1} is shown if and only if i is not more than 50th lowest minimum of LJ_N and $\gamma_{ij}^{N \rightarrow N+1} > 0.1$. For each LJ_N , the global minima as well as some local minima are shown. $MN(n)$ denotes the n th lowest minimum of LJ_N .

are presented in Table 1.

3 Analysis of the Aggregation/Deformation LJ_{6-14} network

The LJ_{6-14} aggregation/deformation network is time-irreversible and reducible. Its states lying in LJ_N for $6 \leq N \leq 13$ are transient. In addition, despite we did not compute the LJ_{15} network, we can assume that a new atom attaches to LJ_{14} as happens for LJ_N , $N \leq 13$, and treat the LJ_{14} component as transient as well. This is equivalent to adding an additional vertex v_{15} to LJ_{6-14} representing LJ_{15} , shooting arcs from every vertex of LJ_{14} to v_{15} , and setting the transition rates along these arcs to μ . We would like to study the relaxation process in the LJ_{6-14} network starting at $M6(2)$, the bicapped tetrahedron local minimum of LJ_6 , that is obtained from the only minimum of LJ_5 by attaching an extra atom. The proposed analysis approach is described in Section 3.1. Central to it is the calculation of the sequence of the expected initial and pre-attachment distributions for each LJ_N , $6 \leq N \leq 14$. The results are presented in Section 3.2. In Section 3.3, the obtained expected initial and the pre-attachment distributions are compared to the invariant distributions. Finally, a structural analysis of local

Table 1: The statistics of the aggregation/deformation LJ₆₋₁₄ network. N is the number of atoms, “# min” is the number of minima, “# ts” is the number of found transition states (Morse index one saddles), “# ts, $i \neq j$ ” is the number of transition states connecting minima mapped to distinct vertices of LJ _{N} , “ $i \neq j, \exists \text{ts}_{ij}$ ” is the number of unordered sets of two vertices of LJ _{N} connected by an edge, i.e., half the number of nonzero off-diagonal entries in the generator matrix L_N , “⟨degree⟩” is the mean vertex degree of the LJ _{N} network, “#min0” is the number of vertices j in LJ _{N} such that there is i in LJ _{$N-1$} such that $\gamma_{ij}^{N-1 \rightarrow N} > 0$.

N	# min	# ts	# ts, $i \neq j$	$i \neq j, \exists \text{ts}_{ij}$	⟨degree⟩	# min0
6	2	3	1	1	1	1
7	4	10	6	5	3	4
8	8	51	30	16	7.5	8
9	21	61	56	45	5.33	15
10	63	938	700	372	22.2	60
11	169	756	722	648	8.54	165
12	505	1582	1525	1410	6.04	487
13	1510	4660	4512	4290	5.98	1450
14	4135	13049	12630	11823	6.11	4109

energy minima is conducted in Section 3.4, and the formation mechanism of configurations with icosahedral packing is investigated.

3.1 Analysis method

For each number of atoms N , $6 \leq N \leq 14$, we compute two probability distributions: the expected probability distribution LJ _{N} after the attachment of the N th atom, and the expected distribution in LJ _{N} right before the attachment of the $(N + 1)$ st atom. We refer to them as *the expected initial and pre-attachment distributions* and denote them by p_0^N and p_e^N respectively.

The expected initial distribution for LJ₆ is $p_0^6 = [0, 1]$, where 0 corresponds to the global minimum M6(1), the octahedron, while 1 corresponds the bicapped tetrahedron M6(2).

The expected pre-attachment distribution for LJ _{N} can be found as follows. We consider two random variables: the continuous random variable T , the attachment time, i.e., the time between the arrivals of two consecutive new atoms, and the discrete random variable S , which indicates the state/vertex immediately before attachment. The joint probability density $f_{S,T}^N(s, t)$ can be expressed as

$$f_{S,T}^N(s, t) = \mathbb{P}^N(S = s|T = t)f_T(t). \quad (8)$$

We assume that T is an exponentially distributed random variable with .pdf $f_T(t) = \mu e^{-\mu t}$.

The probability $\mathbb{P}^N(S = s|T = t)$ can be found from the following considerations. Suppose that the initial probability distribution in LJ₆₋₁₄ is supported within LJ _{N} , where $6 \leq N \leq 14$. Let $p_N(t)$ be the subset of components of the probability distribution corresponding to states of LJ _{N} . Conditioned on the fact that the system remains in LJ _{N} , the probability distribution in LJ _{N} at time t is given by

$$\hat{p}^N(t) = \sum_{k=0}^{M_N-1} (p_0^N \phi_N^k) e^{-\lambda_N^k t} (P_N \phi_N^k)^T, \quad 0 \leq t < T. \quad (9)$$

Here M_N is the number of states in LJ _{N} ; $p_0^N = p^N(0)$ is the initial distribution; $-\lambda_N^k$'s are the eigenvalues of L_N , the restriction of the generator matrix of LJ₆₋₁₄ to LJ _{N} ; ϕ_N^k and $(P_N \phi_N^k)^T$

are the corresponding right and left eigenvectors respectively; P_N is the diagonal matrix with the invariant distribution π_N for LJ_N given by Eq. (3) along its diagonal. The eigenvectors are normalized so that $\Phi_N \Phi_N^T P_N = \Phi_N^T P_N \Phi_N = I$, where $\Phi_N = [\phi_N^0, \dots, \phi_N^{M_N-1}]$ is the matrix whose columns are the right eigenvectors. Hence, right before the arrival of the new atom at time t , $\mathbb{P}(S = s|T = t) = \hat{p}_s^N(t)$, the s th component of $\hat{p}^N(t)$.

Integrating out the attachment time T , we obtain the expected probability distribution at the moment right before the arrival of $(N + 1)$ st atom:

$$\begin{aligned}
p_e^N(s) &\equiv \mathbb{P}^N(S = s) = \int_0^\infty f_{S,T}^N(s, t) dt \\
&= \int_0^\infty \mathbb{P}^N(S = s|T = t) f_T(t) dt \\
&= \int_0^\infty \hat{p}_s^N(t) \mu e^{-\mu t} dt \\
&= \mu \sum_{k=0}^{N-1} (p_0^N \phi_N^k) \left(\int_0^\infty e^{-(\mu + \lambda_N^k)t} dt \right) (P_N \phi_N^k)_s^T \\
&= \sum_{k=0}^{N-1} (p_0^N \phi_N^k) \left(\frac{\mu}{\mu + \lambda_N^k} \right) (P_N \phi_N^k)_s^T.
\end{aligned} \tag{10}$$

Therefore, the expected pre-attachment distribution is given by

$$p_e^N = \mu p_0^N \Phi_N (\mu I - \Lambda_N)^{-1} \Phi_N^T P_N = \mu p_0^N (\mu I - L_N)^{-1}, \tag{11}$$

where $\Lambda_N = \text{diag}\{0, -\lambda_N^1, \dots, -\lambda_N^{M_N-1}\}$.

Once the expected pre-attachment distribution p_e^N is computed using Eq. (11), one can obtain the expected initial distribution for LJ_{N+1} by multiplying the pre-attachment distribution by the $M_N \times M_{N+1}$ transition matrix $\Gamma^{N \rightarrow N+1} = (\gamma_{ij}^{N \rightarrow N+1})$, where $\gamma_{ij}^{N \rightarrow N+1}$ are given by Eq. (7):

$$p_0^{N+1} = p_e^N \Gamma^{N \rightarrow N+1}. \tag{12}$$

Starting from $p_0^6 = [0, 1]$ and using Eqs. (11) and (12), one can compute the sequence of the expected pre-attachment and initial distributions p_e^N and p_0^{N+1} for $6 \leq N \leq 13$ and the pre-attachment distribution p_e^{14} .

3.2 The sequence of the initial and the pre-attachment distributions

We have calculated the expected initial and pre-attachment distributions for the transient LJ_N networks, $6 \leq N \leq 14$, for the range of the attachment rate $10^{-4} \leq \mu \leq 10^4$ and three values of temperatures: $k_B T \equiv \beta^{-1} = 0.06, 0.08, \text{ and } 0.10$. These values of temperatures are below the maximizers of the heat capacity C_v [7] for clusters LJ_N , $7 \leq N \leq 14$ (Fig. 4) corresponding to phase transitions from solid to liquid-like states. The resulting distributions for $10^{-4} \leq \mu \leq 10^4$ are shown in Figs. 5, 6, and 7 for $\beta^{-1} = 0.06, 0.08, \text{ and } 0.10$ respectively. To avoid cluttering near the μ -axis, only those components of the distributions that attain at least 7% likelihood for some values of μ are shown.

Eq. (10) implies that the expected pre-attachment distribution for LJ_N approaches the invariant distribution as $\mu \rightarrow 0$, and approaches the expected initial distribution as $\mu \rightarrow \infty$. Indeed, the factor $\mu(\mu + \lambda_N^k)^{-1}$ tends to zero as $\mu \rightarrow 0$ for all $k \geq 1$, and tends to 1 as $\mu \rightarrow \infty$ for all $k \geq 0$. This is consistent with our results (Figs. 5-7). For all $6 \leq N \leq 14$, the expected pre-attachment distributions for $\mu = 10^{-4}$ are nearly the invariant distributions at the corresponding values of β , while for $\mu = 10^4$, they are nearly the corresponding expected initial distributions. As the attachment rate μ becomes large, the relaxation processes in each LJ_N cluster are limited resulting in broad expected initial and pre-attachment distributions as one can infer from Figs. 5-7.

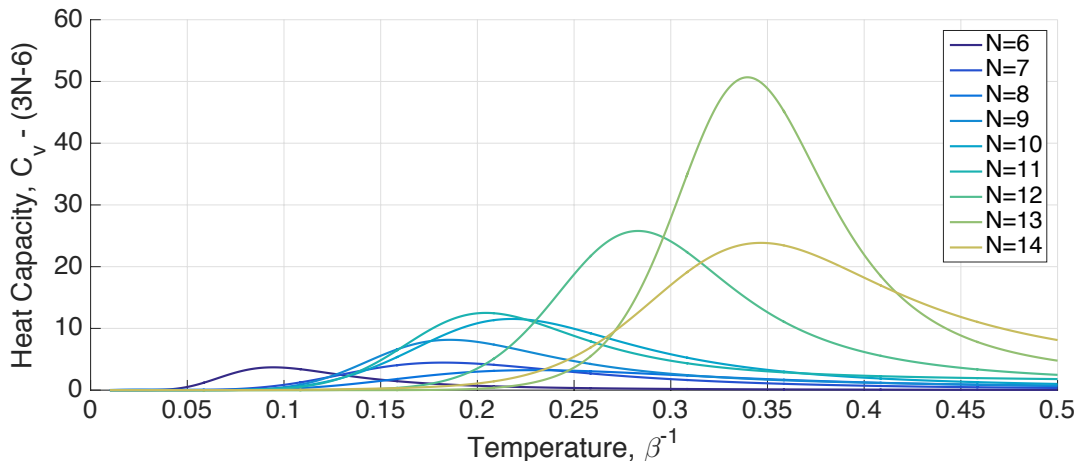


Figure 4: The heat capacities $C_v - (3N - 6)$ for LJ_N networks, $6 \leq N \leq 14$.

The global minima for $7 \leq N \leq 14$ are based on icosahedral packing while the one for $N = 6$ is the octahedron which is an elementary cell of a face-centered cubic crystal. The transitions from the global minima of LJ_N to configurations of LJ_{N+1} , $6 \leq N \leq 14$, happening with probabilities at least 0.1 are illustrated in Fig. 8.

One can observe two types of persisting clusters in Figs. 5 - 7: icosahedral and non-icosahedral. The probabilities of the heirs of the 6-atom octahedron, peaking in the mid-ranges of the attachment rate μ , M7(2), M8(2), M8(3), M9(5), M9(9), and M10(12), are especially prominent for $\beta^{-1} = 0.06$ (Fig. 5). A more complete heritage cascade of non-icosahedral clusters up to $N = 10$ is shown in Fig. 9. The icosahedral heritage cascade is partially displayed in Fig. 10 (partially, as it quickly becomes too broad). Comparing these cascades, we observe that the non-icosahedral one involves only high-energy minima of LJ_{10} : the lowest of them is M10(12). On the contrary, the icosahedral heritage cascade involves all global minima and many other low energy minima for $7 \leq N \leq 14$.

The aggregation process involves two kinds of processes: attachment and relaxation. In order to examine the aggregation process as $\mu \rightarrow \infty$, it is instructive to compare two aggregation processes involving only attachment, one starting from M6(1) and the other one starting from M6(2). The corresponding probability distributions for LJ_N are given, respectively, by

$$a^N := [1, 0]\Gamma^{6 \rightarrow 7} \dots \Gamma^{N-1 \rightarrow N} \quad \text{and} \quad b^N := [0, 1]\Gamma^{6 \rightarrow 7} \dots \Gamma^{N-1 \rightarrow N}. \quad (13)$$

Now, for each state in each LJ_N network, $6 \leq N \leq 14$, we compare the distributions a^N and b^N . Fig. 11 displays the disconnectivity graphs where the states i are plotted red/magenta or blue/black depending on whether $a^N(i) > b^N(i)$ or $a^N(i) < b^N(i)$ respectively. It is evident from Fig. 11 that the probabilities for the global minima of LJ_N , $12 \leq N \leq 14$, to form starting from M6(1) are larger than those starting from M6(2). This is an interesting fact, and we investigate it in more detail.

Let A_N and B_N be the subsets of states of LJ_N defined by

$$A_N := \{i \mid a^N(i) > b^N(i)\}, \quad B_N := \{i \mid a^N(i) < b^N(i)\}. \quad (14)$$

The numbers of states in A_N and B_N as well as the probabilities to find the LJ_N cluster in A_N and B_N assuming the invariant distribution in LJ_N for the temperatures $\beta^{-1} = 0.06, 0.08, 0.10$ are shown in Table 2. The sizes of the sets B_N grow slower than those of A_N , and $|A_N|$ surpasses $|B_N|$ at $N = 10$. Meanwhile, the sets A_N contain only low occupancy states for $N = 7, 8$, and extremely low occupancy (high energy) states for $N = 9, 10, 11$. However, for $N \geq 12$, the sets

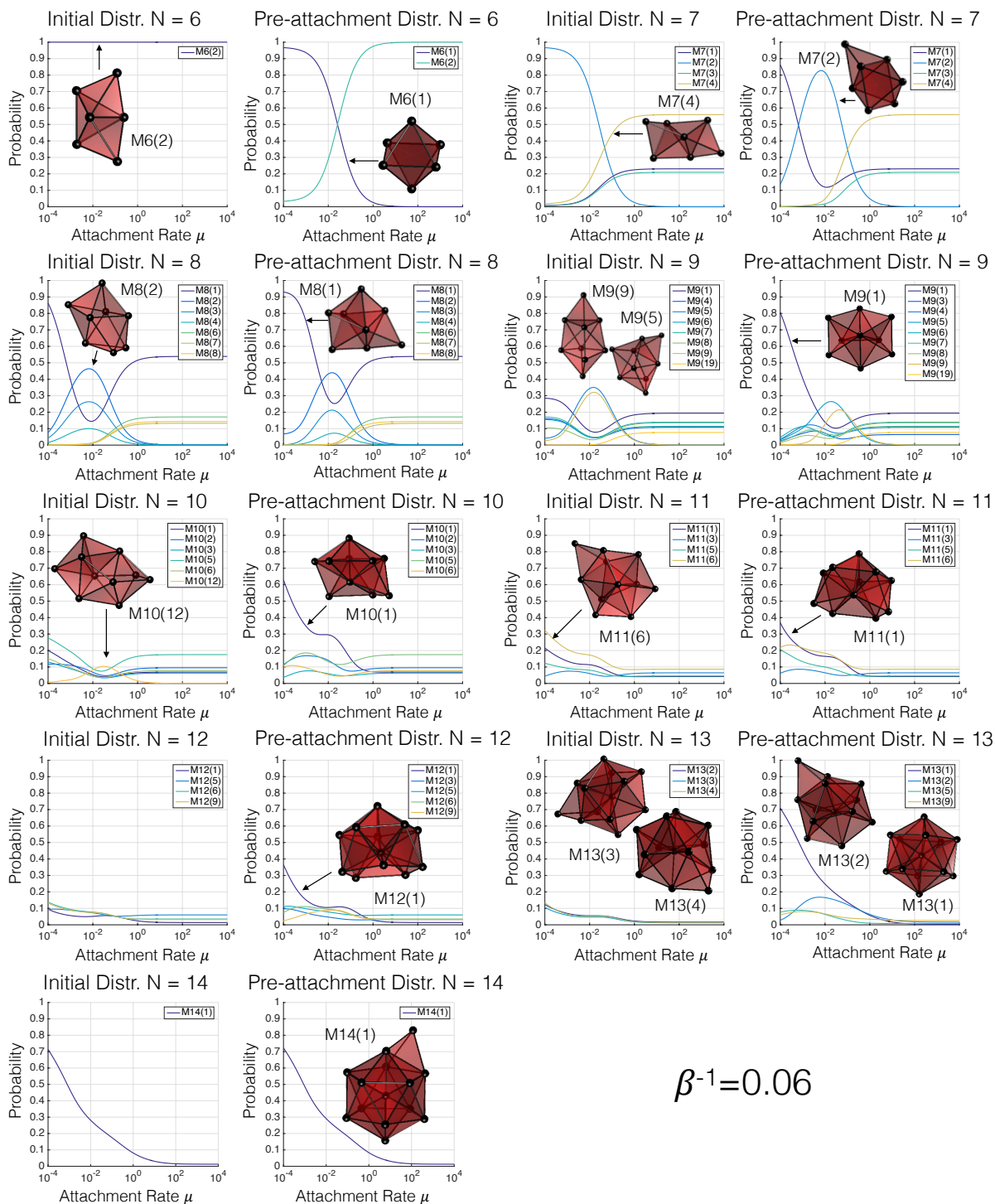


Figure 5: The expected initial and pre-attachment distributions for the aggregation process from $N = 6$ to $N = 14$ atoms at $\beta^{-1} = 0.06$.

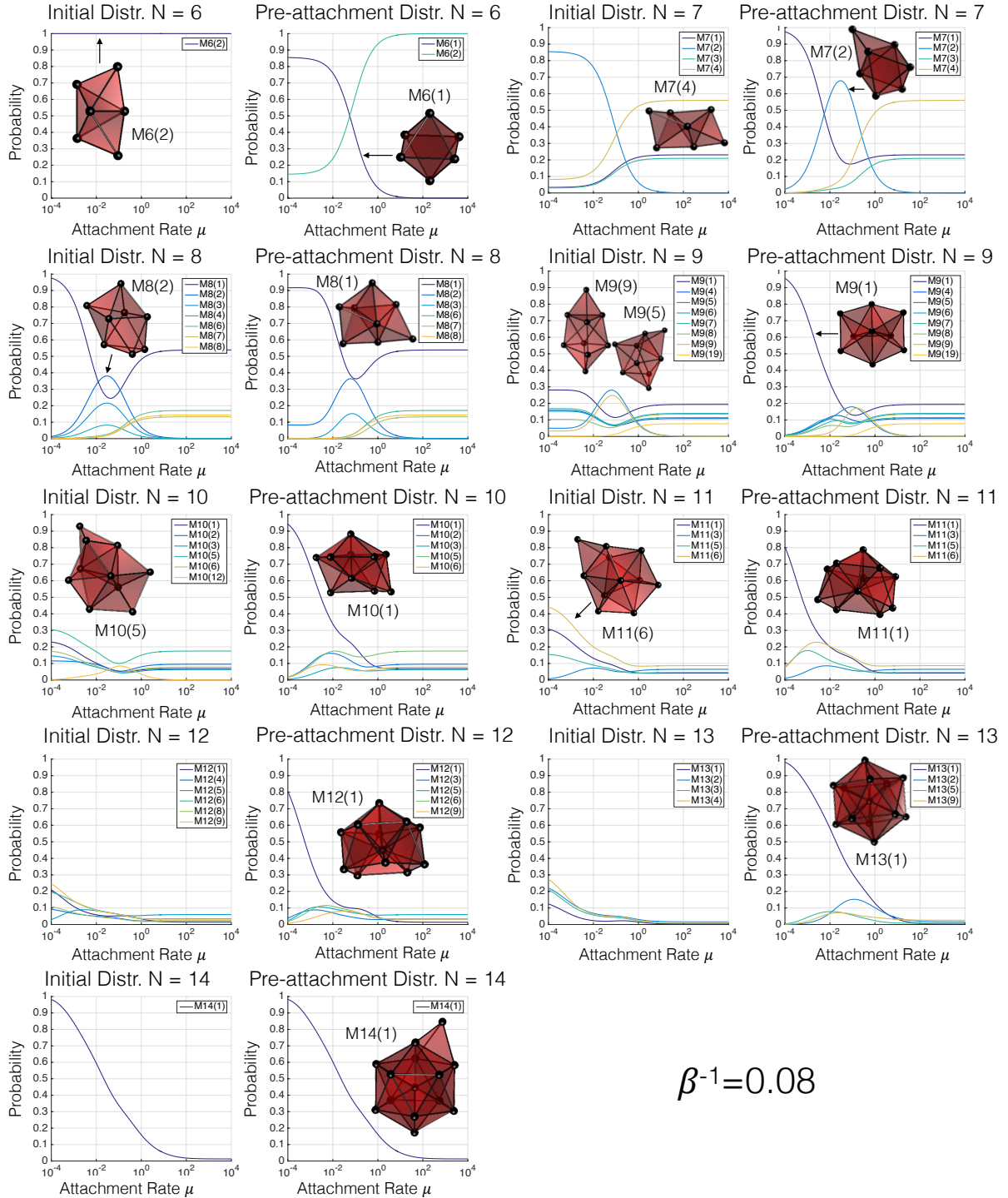


Figure 6: The expected initial and pre-attachment distributions for the aggregation process from $N = 6$ to $N = 14$ atoms at $\beta^{-1} = 0.08$.

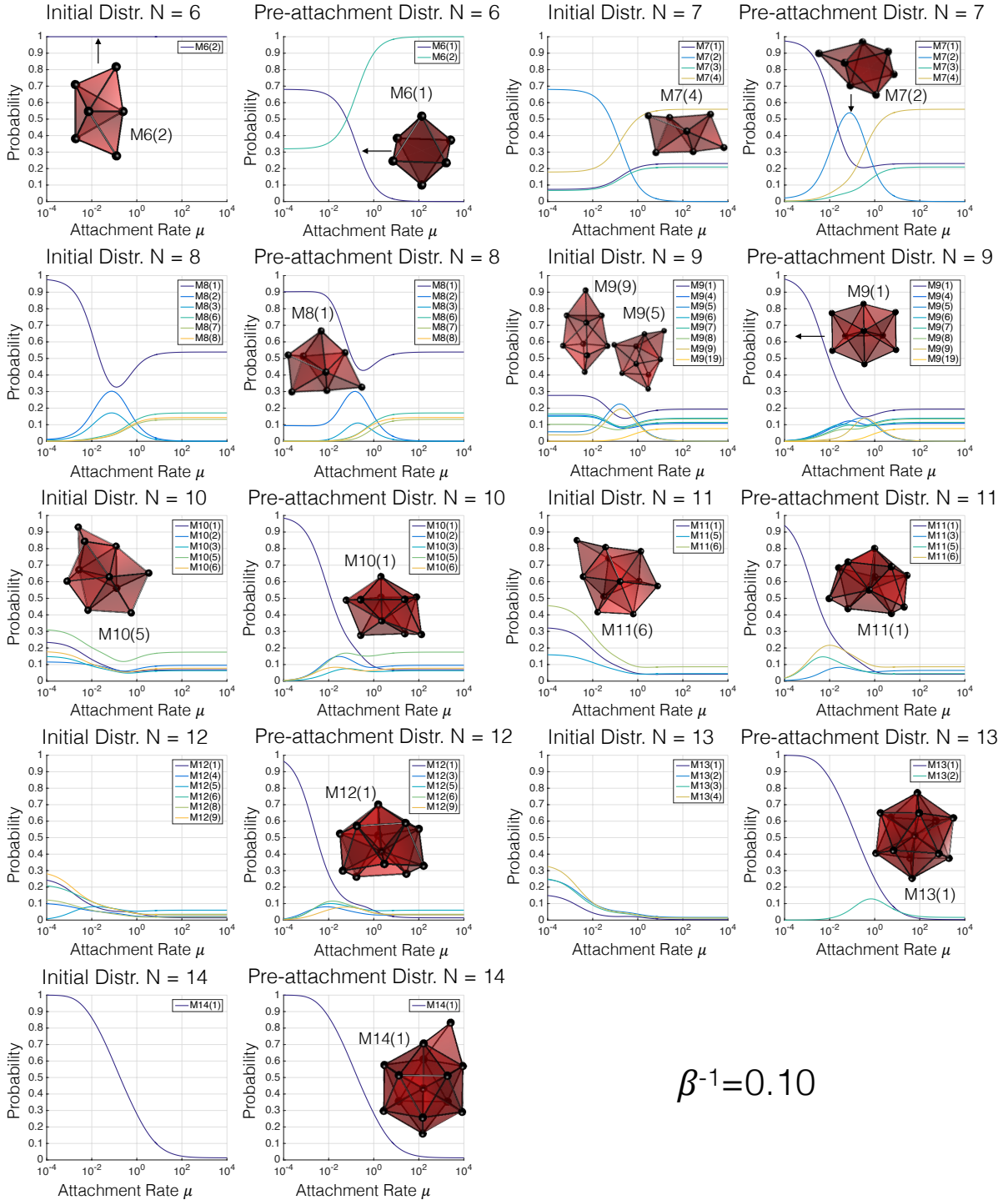


Figure 7: The expected initial and pre-attachment distributions for the aggregation process from $N = 6$ to $N = 14$ atoms at $\beta^{-1} = 0.10$.

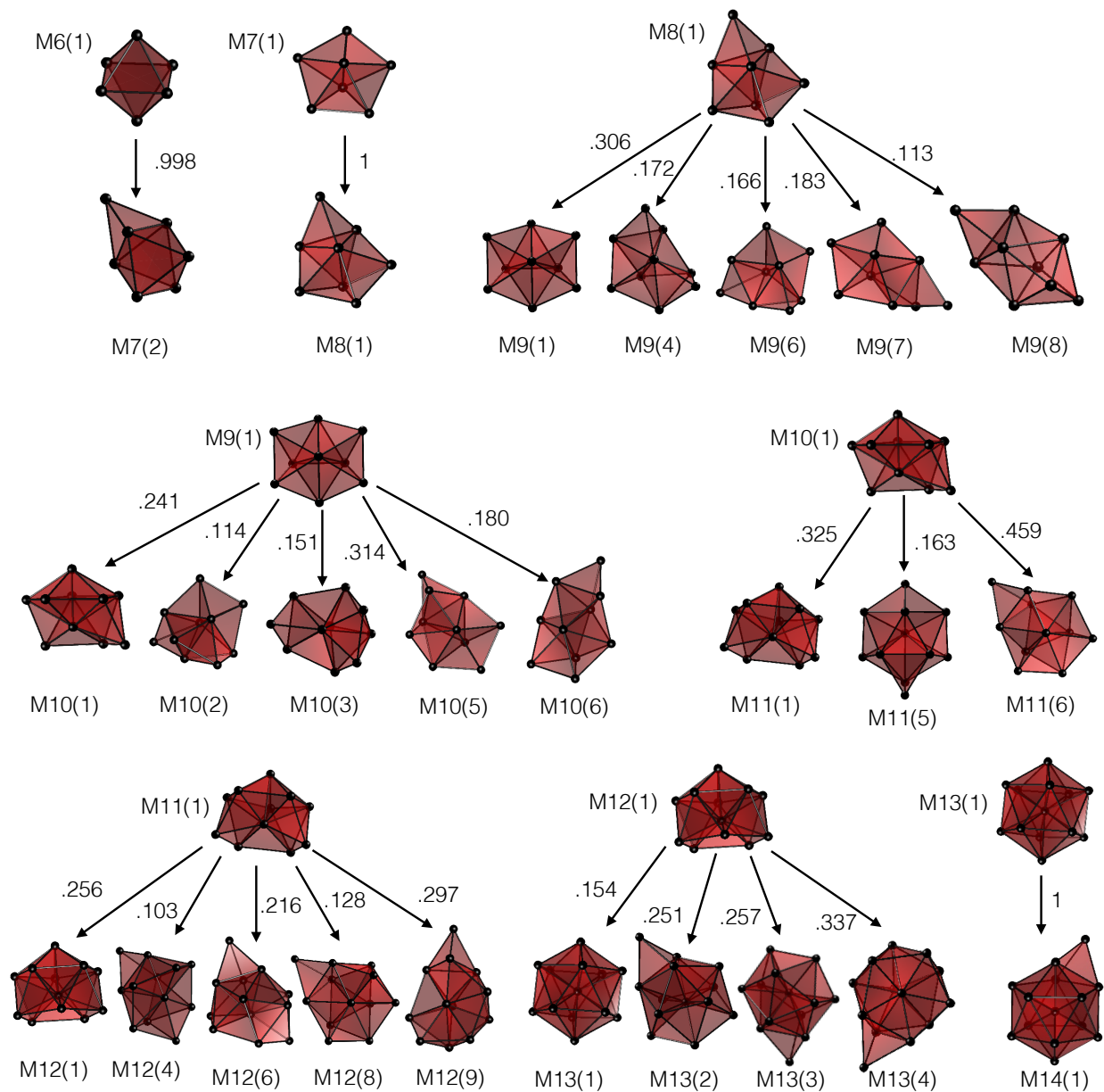


Figure 8: The transitions from the global minima of LJ_N to configurations of LJ_{N+1} , $6 \leq N \leq 14$ happening with probabilities at least 0.1. The numbers next to the arrows indicate the transition probabilities.

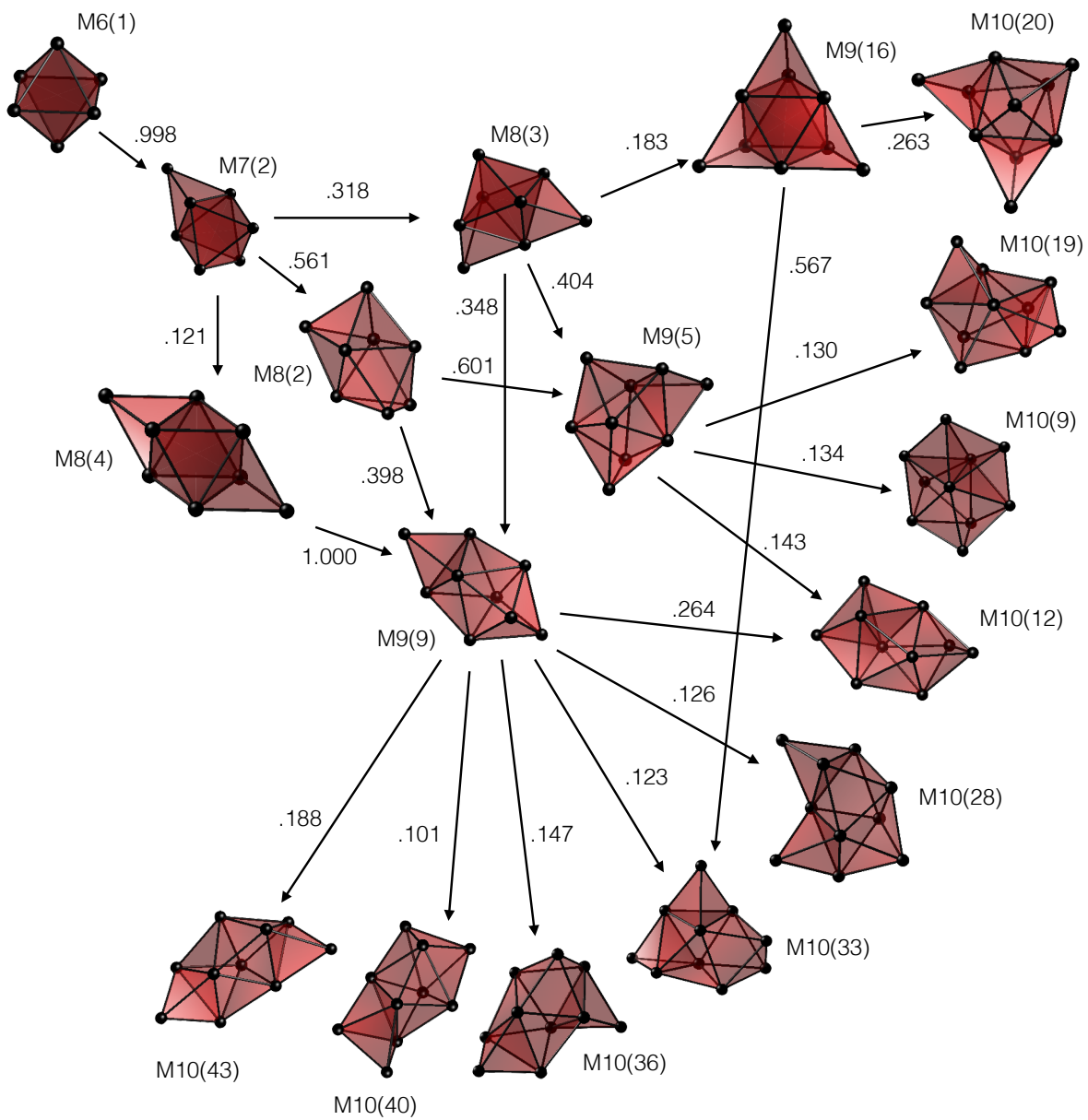


Figure 9: The heritage cascade of the global minimum $M6(1)$ of LJ_6 , the octahedron for up to 10 atoms. All transition probabilities exceeding 0.1 are displayed. The numbers next to the arrows indicate the transition probabilities.

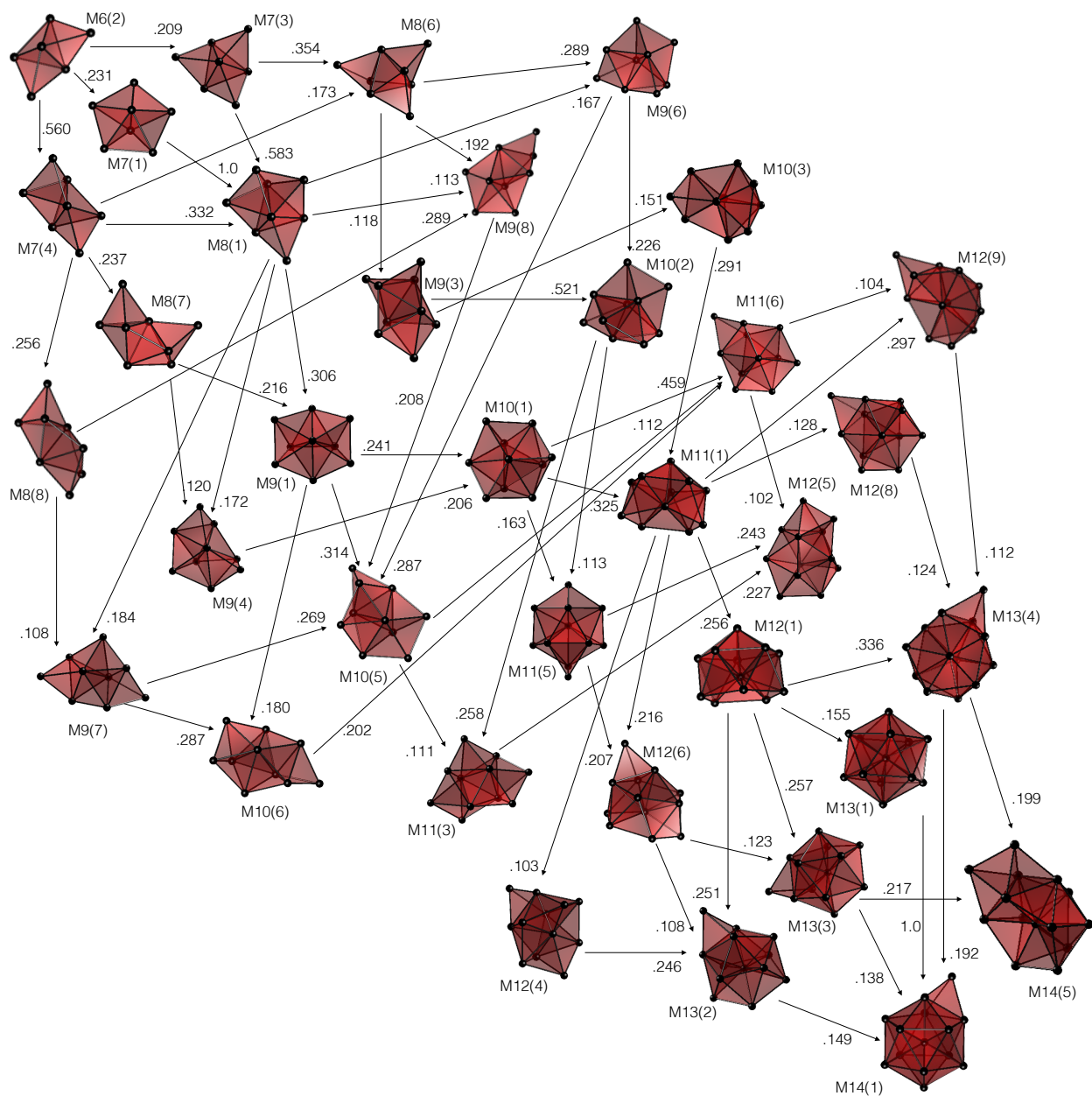


Figure 10: The heritage cascade of the minimum $M6(2)$ of LJ_6 , the bicapped trigonal bipyramid. Only some configurations with probabilities exceeding 0.1 in the expected initial or pre-attachment distributions in Figs. 5-7 and displayed, and only transition probabilities exceeding 0.1 are shown. The numbers next to the arrows indicate the transition probabilities.

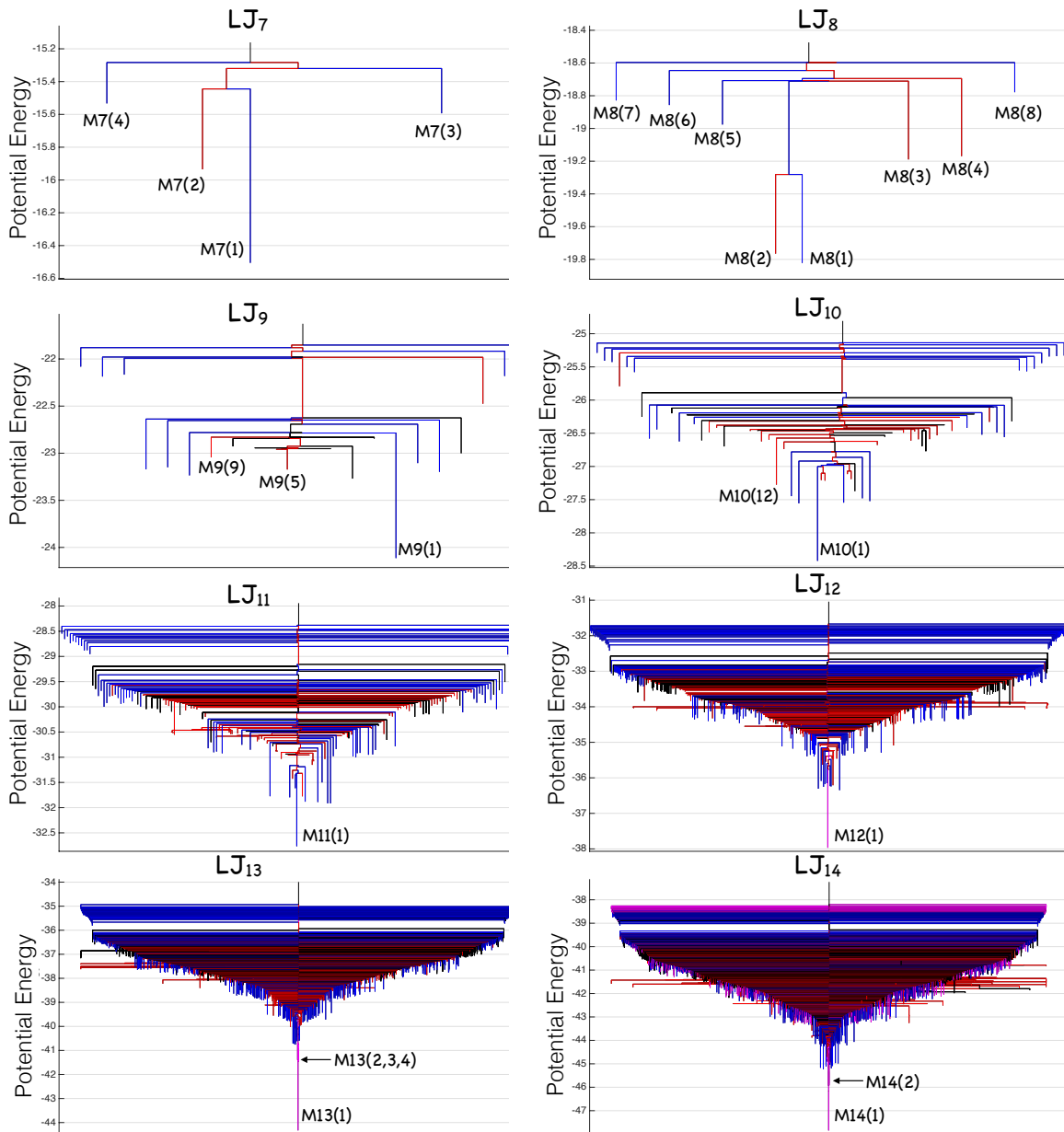


Figure 11: The disconnectivity graphs for $7 \leq N \leq 14$. Blue ($b^N(i) > a^N(i)$) and magenta ($b^N(i) < a^N(i)$) leaves correspond to minima with icosahedral packing. Red ($b^N(i) < a^N(i)$) and black ($b^N(i) > a^N(i)$) leaves correspond to minima with non-icosahedral packing.

A_N acquire the global minima and their probabilities switch to almost one at the considered temperatures.

3.3 Comparison to Invariant Distributions

In this Section, we introduce the normalized root-mean-square (RMS) deviation and use it to compare the computed expected initial and pre-attachment distributions to the invariant distributions for each LJ_N .

Let π be the a probability distribution. The most different from π is the distribution $\chi(i_{\min})$ which assumes 1 at a state $i_{\min} := \arg \min_i \pi_i$ and zeros at all other states. The normalized RMS deviation of a distribution p in LJ_N from π is defined as

$$d_{NRMS}(p, \pi) := \frac{\sqrt{\sum_i (p_i - \pi_i)^2}}{\sqrt{\sum_i (\chi(i_{\min})_i - \pi_i)^2}} \quad (15)$$

The normalized RMS deviations of the expected initial and pre-attachment distributions from the invariant distributions π^N (Eq. (3)) for $6 \leq N \leq 14$ for $\beta^{-1} = 0.06, 0.08$, and 0.10 are shown in Fig. 12 (a),(b),(c) respectively. For all N , as one would expect, $d_{NRMS}(p_0^N, \pi^N)$ and $d_{NRMS}(p_e^N, \pi^N)$ approach $d_{NRMS}^N(b^N)$, the normalized RMS deviation of the asymptotic distribution b^N (Eq. (13)) from π^N , as $\mu \rightarrow \infty$. As $\mu \rightarrow 0$, $d_{NRMS}(p_0^N, \pi^N)$ and $d_{NRMS}(p_e^N, \pi^N)$ approach $d_{NRMS}(\pi^{N-1}\Gamma^{N-1 \rightarrow N}, \pi^N)$ and zero respectively. An interesting fact observed in Fig. 12 is that the deviations $d_{NRMS}^N(p_0^N)$ for $N = 7$ and $9 \leq N \leq 13$ are far from 0 for all attachment rates μ . In particular, $d_{NRMS}(p_0^{13}, \pi^{13})$ is nearly constant. This means that the attachment of a new atom throws invariant distributions for $N = 6$ and $8 \leq N \leq 12$ far away from the invariant distributions in $N = 7$ and $9 \leq N \leq 13$, roughly as far as the distributions b^N . On the other hand, the global minima for $N = 8$ and $N = 14$ are formed with probability one from the global minima of LJ_7 and LJ_{13} respectively (Fig. 8). This explains why the corresponding expected initial distributions are close to the invariant ones for low attachment rates μ . This effect is notably stronger for LJ_{14} because the global minimum of LJ_{13} is much deeper than all other minima in LJ_{13} while the two deepest minima of LJ_8 have close values of energy.

3.4 Structural analysis

Fig. 11 and Table 2 suggest that the 6-atom octahedron M6(1) has a large icosahedral heritage that includes the global minima of LJ_N , $12 \leq N \leq 14$. In this Section, we make the concepts of icosahedral or non-icosahedral packing more precise and quantify the structural transitions from icosahedral to non-icosahedral packings and vice versa during the attachment process.

We will call a local minimum $MN(i)$ of LJ_N *icosahedral* if the following two conditions hold:

1. every atom in $MN(i)$ is a vertex of a tetrahedron, whose vertices are a subset of 4 atoms of LJ_N , and edges are of length $2^{1/6}(1 + \delta)$, where $|\delta| \leq \delta_1$;
2. no two atoms in $MN(i)$ are at distances $2^{1/6}\sqrt{2}(1 + \delta)$, where $|\delta| \leq \delta_2$, or $2^{1/6}d(1 + \delta)$, where $|\delta| \leq \delta_3$. The number d is the distance between the pairs of atoms in M8(2) with 5 nearest neighbors, symmetric with respect to its symmetry plane (Fig. 13 (a)), $d \approx 1.269$.

Otherwise, we call a local minimum $MN(i)$ of LJ_N *non-icosahedral*.

This definition is easy to check automatically. We set $\delta_1 = \delta_3 = 0.1$ and $\delta_2 = 0.05$. The second condition renders minima such as M9(16), a tricapped octahedron (Fig. 9), non-icosahedral. In M9(16), every atom is a vertex of a tetrahedron, however, there is an octahedron in the middle.

Roughly speaking, the majority of local minima in Lennard-Jones clusters can be thought of being assembled out building blocks shown in Fig. 13 (a): tetrahedron, octahedron, M8(2), and hollow icosahedral shell. These blocks can be distorted to avoid cavities/overlaps. For example, M9(5) and M9(9) are capped M8(2), M10(28) is a bicapped M8(2) (Fig. 9), M13(1159) is

Table 2: The numbers of states in the sets A_N and B_N , $7 \leq N \leq 14$ defined by Eq. (14) and the probabilities to find the N-atom cluster in them assuming the invariant distributions in LJ_N.

N, β^{-1}	$ A_N , \mathbb{P}(A_N)$	$ B_N , \mathbb{P}(B_N)$
N = 7	$ A_7 = 1$	$ B_7 = 3$
0.06	3.797e-4	9.996e-1
0.08	4.072e-3	9.959e-1
0.10	1.667e-2	9.833e-1
N = 8	$ A_8 = 3$	$ B_8 = 5$
0.06	6.721e-2	9.328e-1
0.08	8.372e-3	9.163e-1
0.10	9.610e-2	9.039e-1
N = 9	$ A_9 = 10$	$ B_9 = 11$
0.06	2.445e-6	1
0.08	1.679e-4	1
0.10	2.359e-3	9.976e-1
N = 10	$ A_{10} = 38$	$ B_{10} = 25$
0.06	1.522e-7	1
0.08	1.789e-5	1
0.10	3.408e-4	9.996e-1
N = 11	$ A_{11} = 100$	$ B_{11} = 69$
0.06	1.023e-7	1
0.08	1.458e-5	1
0.10	3.666e-4	9.996e-1
N = 12	$ A_{12} = 331$	$ B_{12} = 170$
0.06	1	3.766e-11
0.08	1	4.781e-8
0.10	1	3.568e-6
N = 13	$ A_{13} = 1038$	$ B_{13} = 472$
0.06	1	1.802e-23
0.08	1	6.949e-17
0.10	1	6.398e-13
N = 14	$ A_{14} = 2877$	$ B_{14} = 1257$
0.06	1	4.787e-18
0.08	1	3.870e-13
0.10	1	3.514e-10

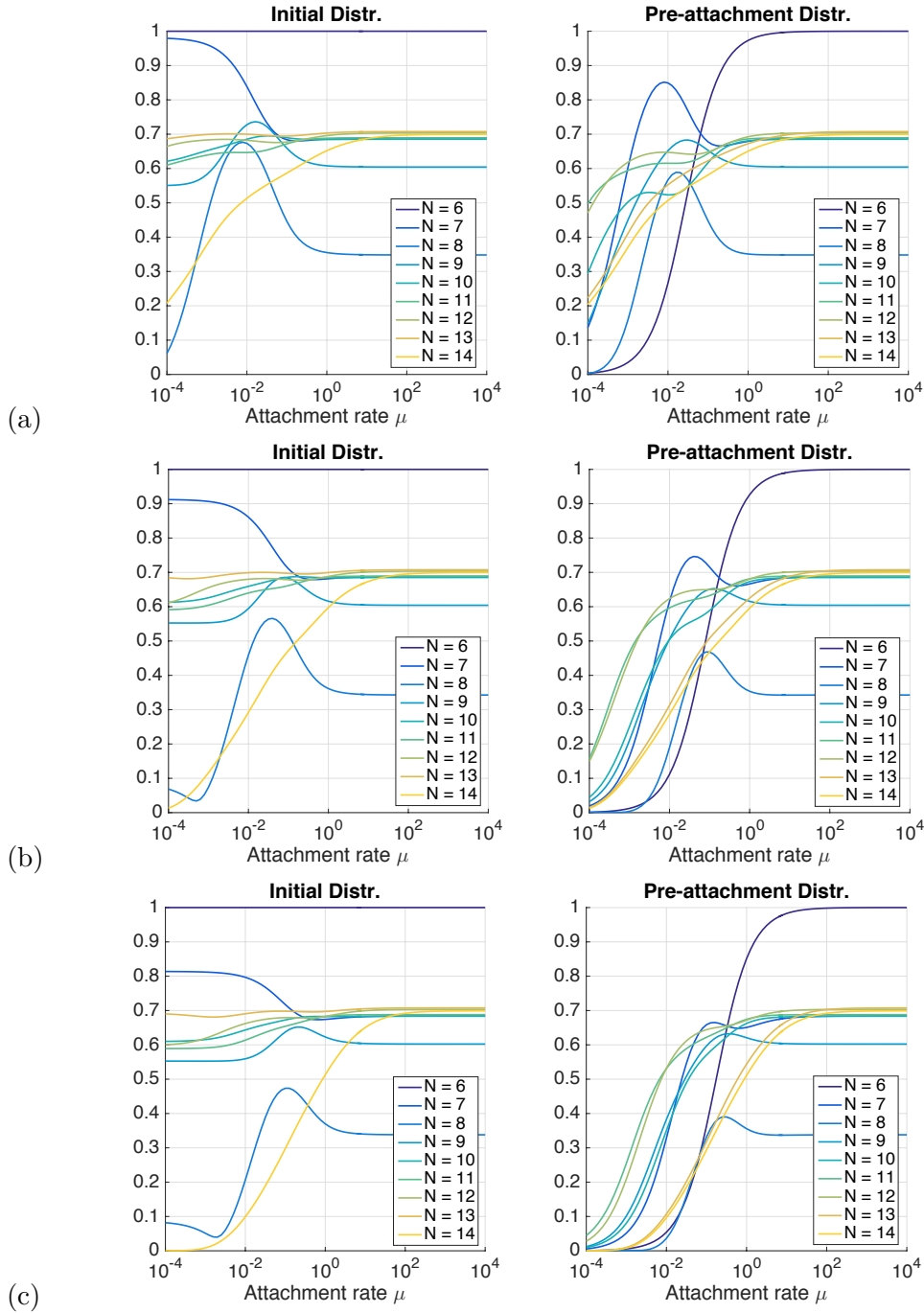


Figure 12: The normalized RMS deviations of the expected initial and pre-attachment distributions from the invariant distributions for $6 \leq N \leq 14$. (a): $\beta^{-1} = 0.06$. (b): $\beta^{-1} = 0.08$. (c): $\beta^{-1} = 0.10$.

a capped icosahedral shell. The numbers of icosahedral and some types of non-icosahedral minima are listed in Table 3. We did not split the types “M6(1) (octahedron) and M8(2)” as their “signature” interatomic distances, $d \approx 1.269$ and $\sqrt{2} \approx 1.414$, are close in comparison with our tolerances δ_i , $i = 1, 2, 3$. The only two non-icosahedral minima of that are not of any of listed types are those of LJ_{14} shown in Fig. 13 (b): M14(43) consists of two distorted hexagons rotated by 30 degrees with respect to each other; M14(3422) has an atom that is not a part of ant tetrahedron. While for $10 \leq N \leq 14$ the numbers of icosahedral minima are less than those of non-icosahedral, one can check that the probabilities to find a cluster in an icosahedral minimum assuming the invariant distribution in LJ_N , $7 \leq N \leq 14$, are very close to one.

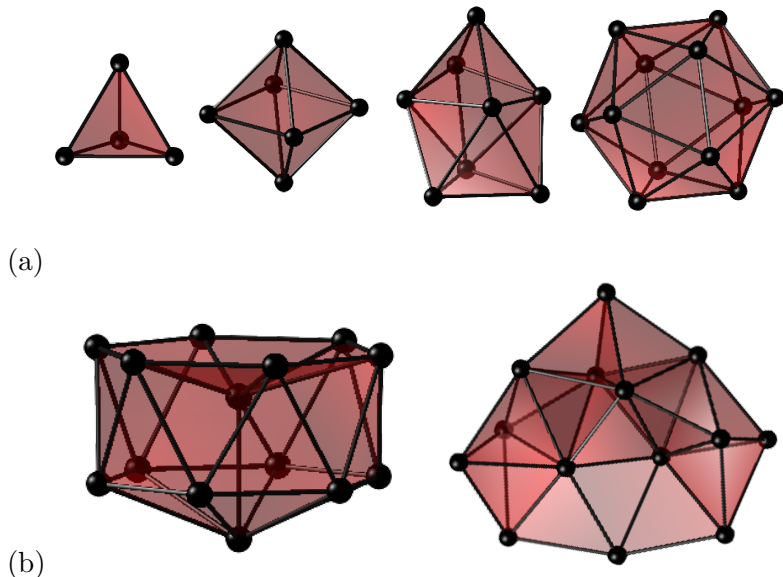


Figure 13: (a): The main building blocks of LJ clusters (left to right): the regular tetrahedron, the octahedron, the M8(2) configuration with the point group D_{2h} of order 8, and the icosahedral shell. (b): The two found minima of LJ_{14} that do not consist of the building blocks above: (left to right) M14(43) can be split to two rotated with respect to each other hexagonal pyramids, M14(3422) contains an atom (the one at the bottom) that is not a part of any tetrahedron.

Transitions probabilities from icosahedral/non-icosahedral minima of LJ_N to icosahedral/non-icosahedral minima of LJ_{N+1} as a result of attachment of a new atom are displayed in Table 4. Evidently, icosahedral minima tend to transition to icosahedral ones, and non-icosahedral minima tent to transition to non-icosahedral ones. However, the transition probabilities from icosahedral to non-icosahedral minima and non-icosahedral to icosahedral ones are nonzero, and the latter ones exceed the former ones by about an order of magnitude, and are significant for $11 \leq N \leq 13$.

Tables 5 and 6 list the numbers of icosahedral and non-icosahedral minima in the distributions a^N and b^N , $6 \leq N \leq 14$, together with their probabilities. The distributions a^N contain both icosahedral and non-icosahedral clusters in comparable proportions for $12 \leq N \leq 14$. In contrast to this fact, the distributions b^N reside primarily on icosahedral minima.

Therefore, the two kinds of processes, relaxation and attachment, involved into the aggregation process up to 14 atoms lead to the formation of icosahedral clusters for $N \geq 11$. Relaxation does so because the global minima of LJ_N , $7 \leq N \leq 14$, are icosahedral. Attachment favors icosahedral minima because icosahedral minima primarily transition to icosahedral ones, while

Table 3: Structure of N -atom clusters. The column “ico” contains the numbers of icosahedral local minima. The column “M6(1) or M8(2)” contains the numbers of local minima involving some interatomic distances characteristic for the octahedron or the M8(2). The column “ico shell” contains the numbers of local minima involving the 12-atom icosahedral shell, capped for LJ₁₃ and bicapped for LJ₁₄. The column “other” contains the numbers of non-icosahedral local minima of none of the above types.

N	ico	M6(1) or M8(2)	ico shell	other
6	1	1	0	0
7	3	1	0	0
8	5	3	0	0
9	11	10	0	0
10	26	37	0	0
11	72	97	0	0
12	175	329	1	0
13	483	1026	1	0
14	1286	2842	5	2

Table 4: Transition probabilities from icosahedral/non-icosahedral local minima of LJ _{N} to icosahedral/non-icosahedral local minima of LJ _{$N+1$} . “ico” and “nico” abbreviate “icosahedral” and “non-icosahedral ” respectively.

$N \rightarrow N + 1$	$\mathbb{P}(\text{ico} \rightarrow \text{ico})$	$\mathbb{P}(\text{ico} \rightarrow \text{nico})$	$\mathbb{P}(\text{nico} \rightarrow \text{ico})$	$\mathbb{P}(\text{nico} \rightarrow \text{nico})$
6 \rightarrow 7	1	0	1.634e-4	9.998e-1
7 \rightarrow 8	9.993e-1	6.702e-4	2.315e-4	9.998e-1
8 \rightarrow 9	1	0	2.540e-4	9.997e-1
9 \rightarrow 10	9.997e-1	2.960e-4	1.118e-3	9.989e-1
10 \rightarrow 11	9.993e-1	7.112e-4	5.002e-3	9.950e-1
11 \rightarrow 12	9.935e-1	6.534e-3	7.440e-2	9.926e-1
12 \rightarrow 13	9.926e-1	7.436e-3	1.575e-1	8.425e-1
13 \rightarrow 14	9.893e-1	1.071e-2	2.272e-1	7.728e-1

non-icosahedral minima start to transition to both, icosahedral and non-icosahedral ones with comparable probabilities for $11 \leq N \leq 13$.

Table 5: The structure of local minima in the distributions a^N (Eq. (13)). The columns “ico” and “nico” contain the numbers of icosahedral/non-icosahedral local minima respectively corresponding to nonzero entries in the distributions b^N , and the columns “ $\mathbb{P}(\text{ico})$ ” and “ $\mathbb{P}(\text{nico})$ ” contain their probabilities.

N	ico	$\mathbb{P}(\text{ico})$	nico	$\mathbb{P}(\text{nico})$
7	1	1.634e-4	1	9.998e-1
8	2	3.949e-4	3	9.996e-1
9	9	8.221e-4	4	9.992e-1
10	23	8.390e-4	22	9.992e-1
11	68	4.336e-3	64	9.957e-1
12	171	1.151e-1	233	8.492e-1
13	475	3.251e-1	709	6.749e-1
14	1264	4.828e-1	1987	5.172e-1

Table 6: The structure of local minima in the distributions b^N (Eq. (13)). The columns “ico” and “nico” contain the numbers of icosahedral/non-icosahedral local minima respectively corresponding to nonzero entries in the distributions b^N , and the columns “ $\mathbb{P}(\text{ico})$ ” and “ $\mathbb{P}(\text{nico})$ ” contain their probabilities.

N	ico	$\mathbb{P}(\text{ico})$	nico	$\mathbb{P}(\text{nico})$
7	3	1	0	0
8	5	9.991e-1	1	8.962e-4
9	11	9.991e-1	2	8.955e-4
10	25	9.990e-1	16	9.969e-4
11	69	9.988e-1	58	1.165e-3
12	171	9.982e-1	220	1.831e-3
13	475	9.978e-1	687	2.203e-3
14	1264	9.967e-1	1955	3.263e-3

4 Concluding remarks

The aggregation/deformation LJ₆₋₁₄ network constructed and analyzed in this work is a model for an isothermal aggregation process, i.e., some amount of energy is taken away from the cluster as it acquires a new atom in such a manner that the mean kinetic energy per atom remains constant. In this work, we had only one control parameter, the attachment rate μ . We assumed that the attachment time was an exponentially distributed random variable with a fixed parameter μ for all N . We did not allow detachments of atoms.

Our results suggest that the primary mechanism of the formation of the 13-atom icosahedron is from the global minimum of LJ₁₄ which is the capped icosahedron: the “cap” atom detaches from the icosahedron. Each atom on the surface of the 13-atom icosahedron has 6 nearest

neighbors, which makes it extremely stable. This would explain the notable peaks in the mass spectra in [12, 17] at $N = 13$. Presumably, a similar mechanism takes place for other clusters with magic numbers of atoms. To check this hypothesis, we will enable atoms to detach from clusters in our future work.

Besides allowing detachments, the study of aggregation processes by means of stochastic networks can be continued in several directions. First, one can continue building LJ_{6-N} aggregation/deformation network for $N > 14$. Due to the exponential growth of the number of local minima in LJ_N with N (Eq. (4)) it will be necessary to use some kind of importance sampling on the set of local minima, e.g., the basin hopping method [30, 31]. For example Wales’s datasets for LJ_{38} [36] and LJ_{75} ¹ contain 100 000 and 593 320 local minima respectively, while the forecast for the numbers of local minima in them according to Eq. (4) are of the orders of 10^{14} and 10^{31} respectively.

Second, one can consider an non-isothermal aggregation and make the attachment rate μ dependent on the current number of atoms in the cluster.

Finally, one can consider aggregation of particles interacting according to various kinds of pair potential as well as aggregation of several kinds of particles assuming that particles of different kinds can be added in a controlled way. Therefore, one can aim at the synthesis of desired configurations by means of self-assembly, while being able to control attachment rate, temperature, and what kind of particle arrives next. The dream of the design by self-assembly inspired the research on the self-assembly of micron-size particles interacting according to a short-range potential [1, 20, 21].

The present work can be considered as the first step toward the goal of generating desired types of clusters by means of controlled aggregation/self-assembly.

Acknowledgement

This work was partially supported by the NSF grant DMS1554907 and the NSF REU grant DMS1359307 at the University of Maryland, College Park.

References

- [1] N. Arkus, V. Manoharan and M. P. Brenner, Minimal Energy Clusters of Hard Spheres with Short Ranged Attractions, *Phys Rev Lett*, **103**,118303 (2009).
- [2] O. M. Becker, and M. Karplus, The topology of multidimensional potential energy surfaces: Theory and application to peptide structure and kinetics, *J. Chem. Phys.* **106** (4), 1495 (1997)
- [3] M. Cameron and E. Vanden-Eijnden, Flows in Complex Networks: Theory, Algorithms, and Application to Lennard-Jones Cluster Rearrangement, *J. Stat. Phys.*, **156**, 3, 427-454 (2014)
- [4] M. K. Cameron, Metastability, Spectrum, and Eigencurrents of the Lennard-Jones-38 Network, *J. Chem. Phys.*, **141**, 184113 (2014)
- [5] M. K. Cameron and T. Gan, Spectral analysis and clustering of large stochastic networks. Application to the Lennard-Jones-75 cluster. *Molecular Simulation*, **42**, 16, 1410-1428 (2016)
- [6] J. M. Carr and D. J. Wales, Folding Pathways and Rates for the Three-Stranded β -Sheet Peptide Beta3s using Discrete Path Sampling, *J. Phys. Chem. B*, **112**, 8760-8769 (2008)
- [7] J. P. K. Doye, D. J. Wales, and M. A. Miller, Thermodynamics and the global optimization of Lennard-Jones clusters, *J. Chem. Phys.* **109**, 8143 (1998)

¹Courtesy of David Wales.

- [8] J. P. K. Doye, D. J. Wales, and M. A. Miller, The double-funnel energy landscape of the 38-atom Lennard-Jones cluster, *J. Chem. Phys.* **110**, 6896 (1999)
- [9] W. E, W. Ren, and E. Vanden-Eijnden, String method for the study of rare events, *Phys. Rev. B*: **66**, 052301 (2002)
- [10] W. E, W. Ren, and E. Vanden-Eijnden, Simplified and improved string method for computing the minimum energy paths in barrier-crossing events, *J. Chem. Phys.*: **126**,164103 (2007)
- [11] W. E and X. Zhou, The gentlest ascend dynamics, *Nonlinearity*, **24**, 1831-1842 (2011)
- [12] O. Eicht, K. Sattler, and E. Recknagel, Magic Numbers for Sphere Packings: Experimental Verification in Free Xenon Clusters, *Phys. Rev. Lett.*, **47**, 16, 1121-1124 (1981)
- [13] O. Eicht and O. Kandler and T. Leisner and W. Mlechle and E. Recknagel, Magic Numbers in Mass Spectra of Large van der Waals Clusters *J. Chem. Soc. Faraday Trans.*, **86**, 2411 (1990)
- [14] J. Farges and M. F. de Feraudy and B. Raoult and G. Torchet, Structure and temperature of rare gas clusters in a supersonic expansion, *Surface Science* **106**, 95, (1981)
- [15] S. N. Fejer and D. J. Wales, Helix Self-Assembly from Anisotropic Molecules, *Phys. Rev. Letters*, **99**, 086106 (2007)
- [16] W. Gao, J. Leng, and X. Zhou, Iterative minimization algorithm for efficient calculations of transition states, *J. Comp. Phys.*, **309**, 6987 (2016)
- [17] I. A. Harris and R. S. Kidwell and J. A. Northby, Structure of charged argon clusters formed in free jet expansion, *Phys. Rev. Lett.*, **53**, 2390 (1984)
- [18] I. A. Harris and K. A. Norman and R. V. Mulkern and J. A. Northby, Icosahedral structure of large charged argon clusters, *Chem. Phys. Lett.*, **130**, 316 (1986)
- [19] G. Henkelman and H. Jonsson, A dimer method for finding saddle points on high dimensional potential surfaces using only first derivatives, *J. Chem. Phys.*, **111**, 7010 (1999).
- [20] M. Holmes-Cerfon, S. J. Gortler, M. P. Brenner, A geometrical approach to computing free-energy landscapes from short-ranged potentials, *Proc. Natl. Acad. Sci.* **110**, 1, E5 - E14 (2013)
- [21] M. Holmes-Cerfon, Sticky-sphere clusters, *Annual Reviews of Condensed Matter Physics*, In press (expected **8**, March 10, 2017).
- [22] H. Jonsson, G. Mills, K. W. Jacobsen, Nudged Elastic Band Method for Finding Minimum Energy Paths of Transitions, in *Classical and Quantum Dynamics in Condensed Phase Simulations*, Ed. B. J. Berne, G. Ciccotti and D. F. Coker, 385 (World Scientific, 1998).
- [23] S. Kakar, O. Bjoernehalm, J. Weigelt, A. R. B. de Castro, L. Troeger, R. Frahm, and T. Moeller, Size-dependent K-edge EXAFS study of the structure of free Ar clusters, *Phys. Rev. Lett.* **78**, 9, 1675-1678 (1997)
- [24] S. I. Kovalenko and D. D. Solnyshkin and E. T. Verkhovtseva and V. V. Eremenko, Experimental detection of stacking faults in rare gas clusters *Chem. Phys. Lett.*, **250**, 309 (1996)
- [25] J. S. Langer, Statistical Theory of the Decay of Metastable States, *Ann. Phys.* **54**, 258-275 (1969)
- [26] V. A. Mandelshtam and P. A. Frantsuzov, Multiple structural transformations in Lennard-Jones clusters: Generic versus size-specific behavior, *J. Chem. Phys.* **124**, 204511 (2006)
- [27] M. A. Miller and D. J. Wales, Isomerization dynamics and ergodicity in Ar₇, *J. Chem. Phys.* **107**, 8568 (1997)
- [28] M. Picciani, M. Athenes, J. Kurchan, and J. Tailleur, Simulating structural transitions by direct transition current sampling: the example of LJ₃₈, *J. Chem. Phys.* **135**, 034108 (2011)

- [29] J. Nocedal and S. J. Wright, Numerical Optimization, Second Edition, Springer, USA, 2006
- [30] D. J. Wales and J. P. K. Doye, Global Optimization by Basin-Hopping and the Lowest Energy Structures of Lennard-Jones Clusters Containing up to 110 Atoms, J. Phys. Chem. A, **101**, 5111-5116, (1997)
- [31] D. J. Wales, *Discrete Path Sampling*, Mol. Phys., **100** (2002), 3285-3306
- [32] B. W. van de Waal, No Evidence for Size-Dependent Icosahedral \rightarrow fcc Structural Transition in Rare-Gas Clusters, Phys. Rev. Lett., **76**, 7, 1083-1086 (1996)
- [33] D. J. Wales, "Energy Landscapes: Applications to Clusters, Biomolecules and Glasses", Cambridge University Press, 2003
- [34] D. J. Wales, *Energy landscapes: calculating pathways and rates*, International Review in Chemical Physics, **25**, 1-2, 237-282 (2006)
- [35] D. J. Wales, Energy Landscapes of Clusters Bound by Short-Ranged Potentials, J. Chem. Phys. and Phys. Chem., **11**, 12, 2491-2494 (2010)
- [36] <http://www-wales.ch.cam.ac.uk/CCD.html>
- [37] J. Zhang and Q. Du, Shrinking dimer dynamics and its applications to saddle point search, SIAM J. Numer. Anal., **50**, 4, 1899-1921 (2012)